Solvation structure engineering of weakly coordinating sulfonamide electrolytes for 4.6 V lithium metal batteries

Lea Pompizii[a], Mingliang Liu[a], Leonie Braks[a], Timur Ashirov[a], Tianhong Zhou[a], Mounir Mensi[b], Dongmin Park[c], Jang Wook Choi[c*], Ali Coskun[a*]

[a]Department of Chemistry, University of Fribourg, Chemin de Musee 9, Fribourg 1700, Switzerland

[b]Institute of Chemical Sciences and Engineering (ISIC), École Polytechnique Fédérale de Lausanne, Sion, 1950, Switzerland

[c]School of Chemical and Biological Engineering and Institute of Chemical Processes, Seoul National University, Seoul, 08826, Republic of Korea

Corresponding Author

* Ali Coskun – Email: ali.coskun@unifr.ch

* Jang Wook Choi – Email: jangwookchoi@snu.ac.kr

ABSTRACT A series of trifluoromethanesulfonamide solvents were synthesized with systematically controlled ring size (4-6) at the *N*-terminal to tune their steric and electronic properties to realize enhanced contact ion pairs for the formation of anion-derived SEI and compatibility with the NMC811 cathode. Comparative analyses of electrolytes revealed that the 1.6 M LiFSI 1-azetidine trifluoromethanesulfonamide (AzTFSA) electrolyte presents the ideal combination of steric and electronic effects along with high oxidation stability up to 5 V and a Coulombic efficiency of 99.2% in Cu-Li half-cells at 1mA cm^{-2} and 1 mAh cm^{-2}. The corresponding full cells using 20 μm of Li foil paired with the NCM811 cathode by a negative and positive capacity ratio (N/P) of 2.5, achieve 80% capacity retention after 150 cycles at 0.5 C. Even at a high charge cut-off voltage of 4.6 V, the Li|NCM811 full cell still realizes 92% retention at 0.5 C after 100 cycles.

TOC GRAPHICS

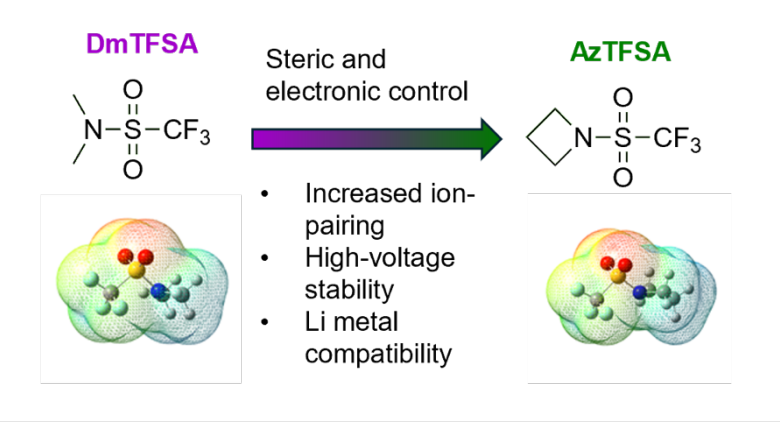

The growing demand for high energy density batteries led to increasing focus on the Li metal anode, which has an extremely high theoretical specific capacity of 3860 mA h g^{-1} compared to that of graphite[1-4]. However, the detrimental Li dendrite growth, low Coulombic efficiency, short cycle life, and side reactions with the electrolyte hinder the practical application of the Li metal anode. In particular, the low thermodynamic stability of the electrolytes towards the Li metal anode leads to uncontrolled side reactions, which in turn leads to the formation of inhomogeneous and unstable solid-electrolyte interface (SEI) causing nonuniform Li deposition, thus promoting the growth of lithium dendrites as well as the accumulation of dead Li[5-7], which leads to severe performance degradation of the Li metal battery (LMB) during cycling[8]. In this direction, electrolyte engineering emerged as a promising approach to control the composition of SEI, for which various solvent, salt, and additive combinations have been investigated to form an anion-derived inorganic-rich SEI[9-13]. While linear and cyclic carbonate ester electrolytes have been successfully applied in conventional Li-ion batteries, when paired with Li metal anode, they form an organic-rich, non-uniform, and mechanically weak SEI, which exacerbates lithium dendrite formation and electrolyte decomposition[14]. Ether electrolytes, on the other hand, show good compatibility with the Li metal anode due to their high reductive stability (high LUMO). The main issue is their limited voltage stability (below 4 V), which hinders pairing with the high-voltage NMC811 cathode[15,16]. Fluorosulfonamides emerged as promising solvents that mimic commonly used salts such as LiFSI and LiTFSI, combining excellent high-voltage stability with Li metal compatibility to enhance LMB's

performance and safety[17, 18]. However, owing to their complex synthesis and cost, there are a rather limited number of fluorosulfonamide-based solvents reported in the literature.

The solvation structure of the electrolytes has been shown to have a profound impact on the SEI composition and morphology[19] and can be identified in three ways, namely solvent-separated ion pairs (SSIP), contact ion pairs (CIP), and aggregated ion pairs (AGG). Both CIP and AGG can induce the formation of an inorganic-rich SEI[20] as the anion is located close to $Li^{+,}$ and the LUMO level is shifted from the solvent to the anion so that it gets preferentially reduced[21]. The formation of CIP and AGG can be induced by increasing the salt concentration, adding diluents, or modulating the electronic properties of the solvent molecules by introducing electron-withdrawing groups and/or by controlling the steric properties of solvents[3, 22-27]. Highly concentrated electrolytes (HCEs) reduce the amount of free solvent and increase the ratios of CIP and AGG owing to their high salt content in the electrolyte [28]. However, HCEs suffer from high viscosity, poor wettability, and high cost. Localized high-concentration electrolytes (LHCEs) overcome these drawbacks by introducing a non-solvating co-solvent/diluent, enabling a similar solvation structure to HCEs at lower salt concentrations[29]. While the use of LHCEs enabled high CEs and enhanced cycle life, it has been recently demonstrated that they exhibit limited calendar life owing to the corrosion of the Li metal anode[30]. More recently, weakly coordinating electrolytes (WCEs) have emerged as promising candidates in this direction, which involves the gradual decrease in the solvation power, without over-fluorination, of a solvent through molecular structure control to increase the CIP and AGG content[3, 31, 32]. WCEs also offer significant gains in terms of ionic conductivity

over LHCEs and HCEs. In this direction, the targeted molecular functionalization approach has been successfully applied to a variety of solvent molecules[33, 34]. Extending/shortening the chain length of ethylene-bridge and/or methyl groups of DME, as well as the introduction of -F atoms commonly applied to form WCEs through steric/electronic control[11]. Ideally, solvent fluorination should be kept to a minimum due to the additional challenges that arise from the recycling of such solvents[35].

Salt-like sulfonamide solvents as WCEs can be grouped into two classes mimicking LiFSI (fluorosulfonamides) or LiTFSI (trifluoromethylsulfonamides). The modification of the *N*-termini enables the formation of new electrolyte solvents[36-38]. The application of dimethyl trifluoromethyl sulfonamide (DmTFSA) electrolyte with a high-voltage NMC811 cathode and Li metal anode by Xue and coworkers[17] triggered significant interest and further structural modification of these weakly solvating solvents. Despite being known as high-voltage tolerant solvents, there is limited understanding of their solvation structure and its correlation with the SEI composition and morphology along with the electrochemical performance. In this work, we systematically varied the size of the functional groups at the *N*-terminus in trifluoromethanesulfonamides to tune both steric and electronic properties of these weakly solvating solvents and investigated their impact on the electrolyte solvation structure and electrochemical performance. We systematically studied the structure-property relationship of different cyclic amine substituents in trifluoromethanesulfonamides, namely, dimethylamine (DmTFSA), azetidine (AzTFSA), pyrrolidine (PyTFSA), piperidine (PiTFSA), and morpholine (MoTFSA). Dissolution of bis(fluorosulfonyl)imide (LiFSI) salt in these

solvents results in electrolytes with ultra-high oxidation tolerance up to 5 V. Among all the electrolytes, AzTFSA provides ideal steric and electronic control to enhance CIP and AGG formation due to its low Li^+ solvation ability and structural rigidity, rendering less conformational freedom towards Li^+ solvation. This enables preferential anion reduction at the Li metal anode and the formation of a LiF-rich, inorganic, and stable SEI layer. 1.6 M AzTFSA electrolyte showed enhanced compatibility with the Li metal anode and a wide electrochemical window, which enables stable cycling of NMC811 at a high cut-off voltage of 4.6 V with a limited 20 μm Li metal anode (N/P = 2) and 20 μL of electrolyte at 0.5C with a capacity retention of 90% after 100 cycles.

The DmTFSA can be modified at the *N*-terminus or the *S*-terminus[39, 40]. We reasoned that the introduction of bulky and rigid amine substituents could not only impact the electron density at the sulfonamide oxygen but also modify the solvation structure through the steric crowding in the first solvation shell, thus favoring the formation of CIP and AGG. Accordingly, we synthesized a series of trifluoromethanesulfonamide solvents, namely, DmTFSA, AzTFSA, PyTFSA, PiTFSA, and MoTFSA. AzTFSA was synthesized from the HCl salt of azetidine instead of the free amine. The ^1H, and ^{19}F-NMR analyses prove the successful synthesis of the solvents (Figures S1-S9). We have recently demonstrated that electrostatic potential (ESP) surface map visualization data can be correlated to the solvation power of the solvents[11]. To probe the impact of the substituents, we calculated the ESP minimum of the synthesized sulfonamide solvents by density functional theory (Figure 1a). The ESP_{min} values increase from MoTFSA < DmTFSA < AzTFSA < PiTFSA < PyTFSA (Figure 1a). Based on their

ESP_{min} values, these solvents can be classified as weakly solvating solvents. Except for the morpholine with an additional O atom in the cycle, these results suggest smaller substituents on the N-terminus lead to lower ESP_{min} values (Table S1). It should, however, be noted that ESP calculations do not consider the steric effects of the substituents on the Li^+ solvation ability, thus they should be considered together. The electrolytes were prepared by dissolving 1.6 M LiFSI in the electrolyte solvent, which was determined to be the solubility limit, except for the PiTFSA, for which only 1 M LiFSI can be dissolved. The linear sweep voltammetry (LSV) analysis confirmed the high oxidative stability of all the solvents as previously reported for DmTFSA (Figure 1b). Notably, the ionic conductivity decreases with increasing ring size of the substituent on the nitrogen (Figure 1c), thus demonstrating the significant effect of the N-substituents on the ionic conductivity of the electrolyte. The transference number of the electrolyte reaches a maximum for AzTFSA and PiTFSA (Figure 1d). MoTFSA showed negligible ionic conductivity, thus suggesting the negative impact of the large ring size and the O atom on the morpholine ring. Accordingly, MoTFSA was excluded from the subsequent characterizations.

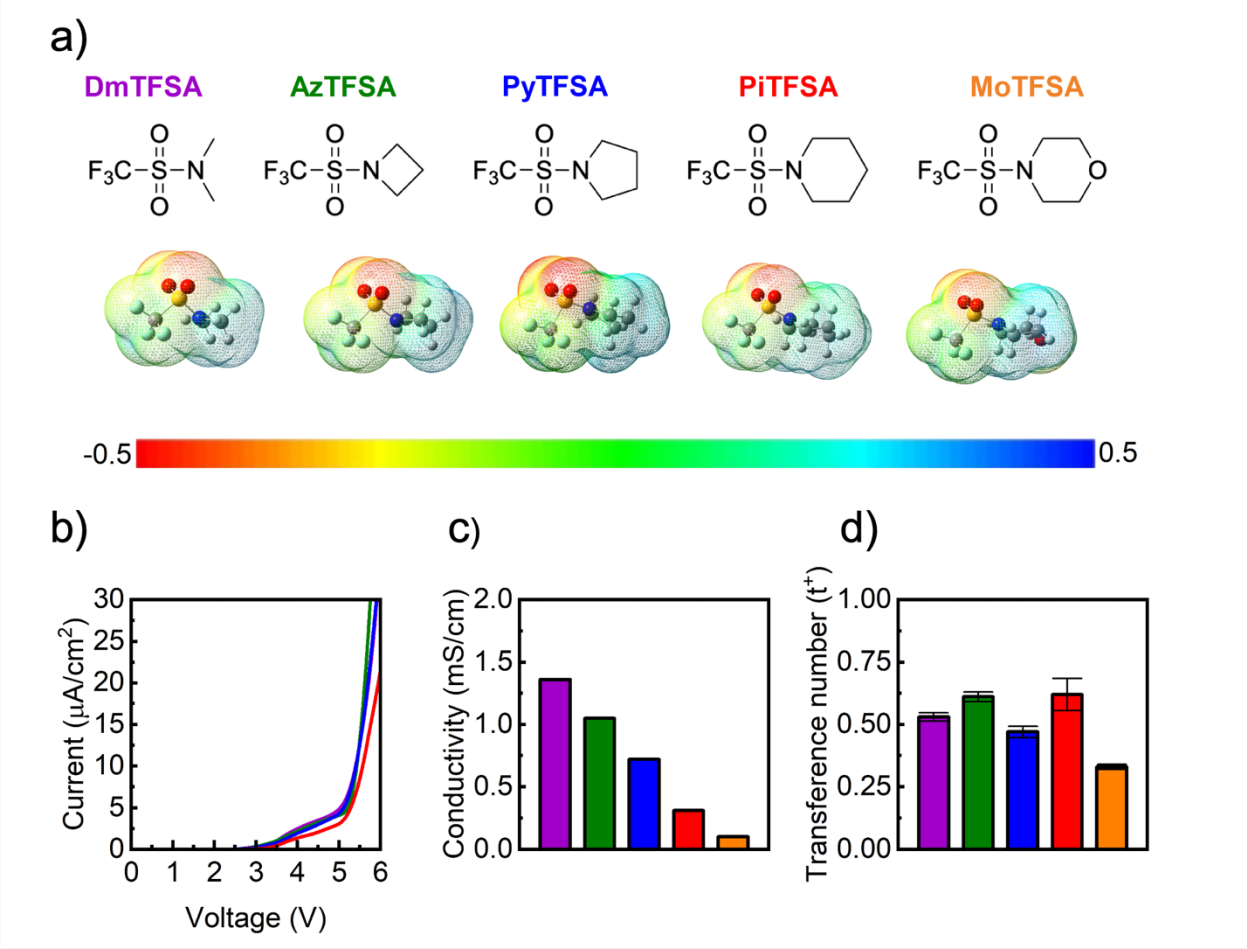

Figure 1. (a) Molecular structure and ESP mapping of sulfonamide solvents. (b) Oxidation stability of electrolytes in Li|Al half cells obtained from LSV. (c) Ionic conductivity of sulfonamide electrolytes measured in coin cell configuration. (d) Li^+ transference number of sulfonamide electrolytes.

In order to test the ability of the modified sulfonamide electrolytes to enable reversible Li plating and stripping, the modified Aurbach test was performed[41]. The Aurbach test confirms the high Coulombic efficiency (CE) of AzTFSA, DmTFSA and PyTFSA electrolytes compared to that of PiTFSA (Figure 2a). The CE of the electrolytes was also tested in Cu-Li cells by

plating and stripping at a capacity of 1 mAh cm^{-2} at 1 mA cm^{-2} after preconditioning of 10 cycles at 0.05 mA cm^{-2} (Figure 2b)[15]. Both AzTFSA and DmTFSA electrolytes were able to deliver CE values over 99% during the entire cycling. However, the DmTFSA electrolyte showed a much earlier cell failure. In addition, PiTFSA solvent showed a high overpotential for Li plating and stripping and an average CE below 98%. The high CE values of DmTFSA, AzTFSA, and PyTFSA prompted us to further study their interfacial stability with Li metal, and electrochemical impedance spectroscopy (EIS) was performed in a Cu-Li cell and cycled at 0.5 mA cm^{-2} with a cut-off capacity of 0.5 mAh cm^{-2} (Figure S10). The impedance evolution clearly shows that in the AzTFSA electrolyte a stable interface is obtained after the first 40 cycles whereas DmTFSA and PyTFSA showed continuously increasing impedance. To further verify the compatibility of AzTFSA, DmTFSA and PyTFSA with Li metal, asymmetric Li-Cu cells were assembled. After a precycling step, 5 mAh cm^{-2} of Li was plated on Cu and subsequently stripped and plated with 1 mA cm^{-2} and a cut-off capacity of 1 mAh cm^{-2} (Figure 2c). AzTFSA and DmTFSA both show stable overpotential for 200 h. Afterwards, the overpotential for DmTFSA increases drastically compared to AzTFSA. PyTFSA electrolyte showed more severe overpotential growth and cell failure after 200 h. Cyclic voltammetry (CV) was performed to understand the reductive stability of the electrolytes. Two distinctive peaks are visible in the CV plots of DmTFSA and AzTFSA (Figure S11). The first peak corresponds to LiFSI decomposition, which occurs around 2.4 V to 1.4 V, depending on the solvent system[42-45]. The electrolyte decomposition occurs at a similar voltage for all the electrolytes before 0 V. However, AzTFSA shows a lower decomposition current compared to DmTFSA

during the first cycle as well as after the subsequent cycles, suggesting better interfacial stabilization.

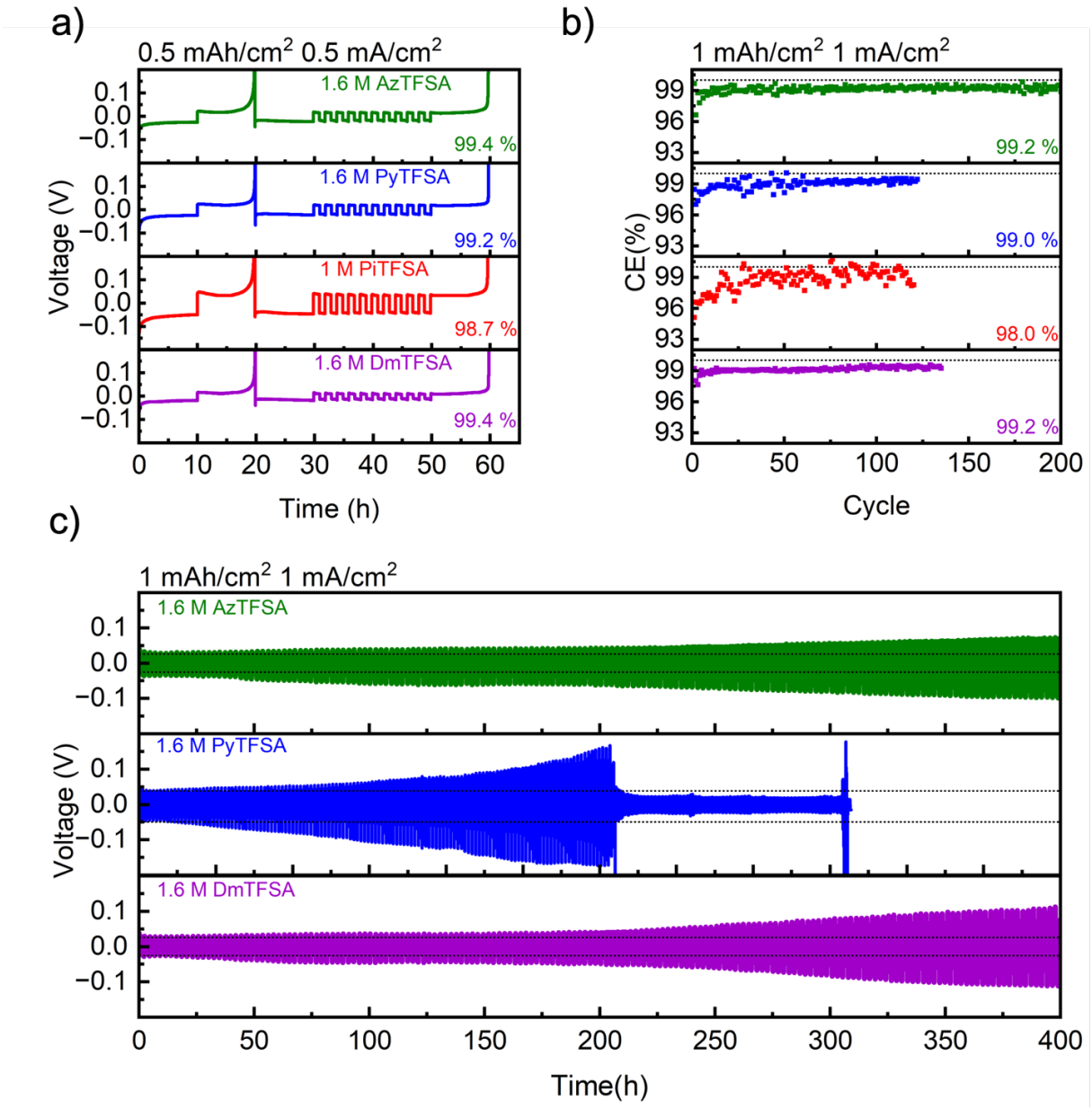

Figure 2. (a) Average CE test of sulfonamide electrolytes by Aurbach method. (b) CE test of Li||Cu asymmetric cells using different electrolytes at 1 mA cm^{-2} with a cutoff capacity of 1 mAh cm^{-2}. (c) Voltage–time profiles of Li||Li symmetric cells with different electrolytes.

The morphology of the plated Li metal on Cu substrates with 1.6 M DmTFSA, 1.6 M AzTFSA, 1.6 M PyTFSA electrolytes was imaged by scanning electron microscopy (SEM). 5 mAh cm^{-2} of Li was deposited on Cu substrate, the Li metal plated in 1.6 M AzTFSA electrolyte showed uniform Li grain morphology with a good surface coverage (Figure S12). Compared to 1.6 M DmTFSA and 1.6 M PyTFSA, the deposited Li grains were large and densely packed. The Li morphology evolution during cycling was studied by depositing a Li metal capacity of 1 mAh cm^{-2} at 0.5 mAh cm^{-2} for 20 cycles. The plated Li metal retained its large and uniform grain size and did not show dendrite growth (Figure S13). FT-IR analysis was performed to gain further insights into the solvation structure of the sulfonamide electrolytes. The intensity of the free FSI^- peak at 1370 cm^{-1} gradually decreased from PyTFSA, DmTFSA to AzTFSA, suggesting increasing ion pairing (Figure 3b)[46]. Raman spectroscopy analysis was carried out for 1.6 M DmTFSA, 1.6 M AzTFSA, and 1.6 M PyTFSA electrolytes (Figure 3c). Meanwhile the Raman band of the S-N-S mode of FSI- and the -CF_3 of the sulfonamide solvent are located at similar wavenumbers in the range of 720 cm^{-1} to 750 cm^{-1}, 1.6 M DmTFSA and 1.6 M AzTFSA clearly show the presence of new peaks at 743 cm^{-1} and 753 cm^{-1}, which corresponds to AGG and CIP formation[15, 34]. The FT-IR and Raman data collectively suggest the highest AGG and CIP formation in the 1.6 M AzTFSA electrolyte in line with the Li-Li symmetric cell results followed by the DmTFSA. Mostly overlapping peak shapes of the PyTFSA and 1.6 M PyTFSA in the Raman spectra (Figure 3c), pointed to the limited formation of CIP and AGG owing to its higher Li^+ solvation power compared to both AzTFSA and DmTFSA. NMR analysis was performed to further probe the solvation structure of the electrolytes. ^{7}Li NMR shows the

largest upfield shift for 1.6 M PyTFSA and the smallest for 1.6 M DmTFSA (Figure 3d). A larger upfield shift can originate from either stronger solvation power towards Li^+ by the solvent or enhanced Li^+-FSI^- interaction.

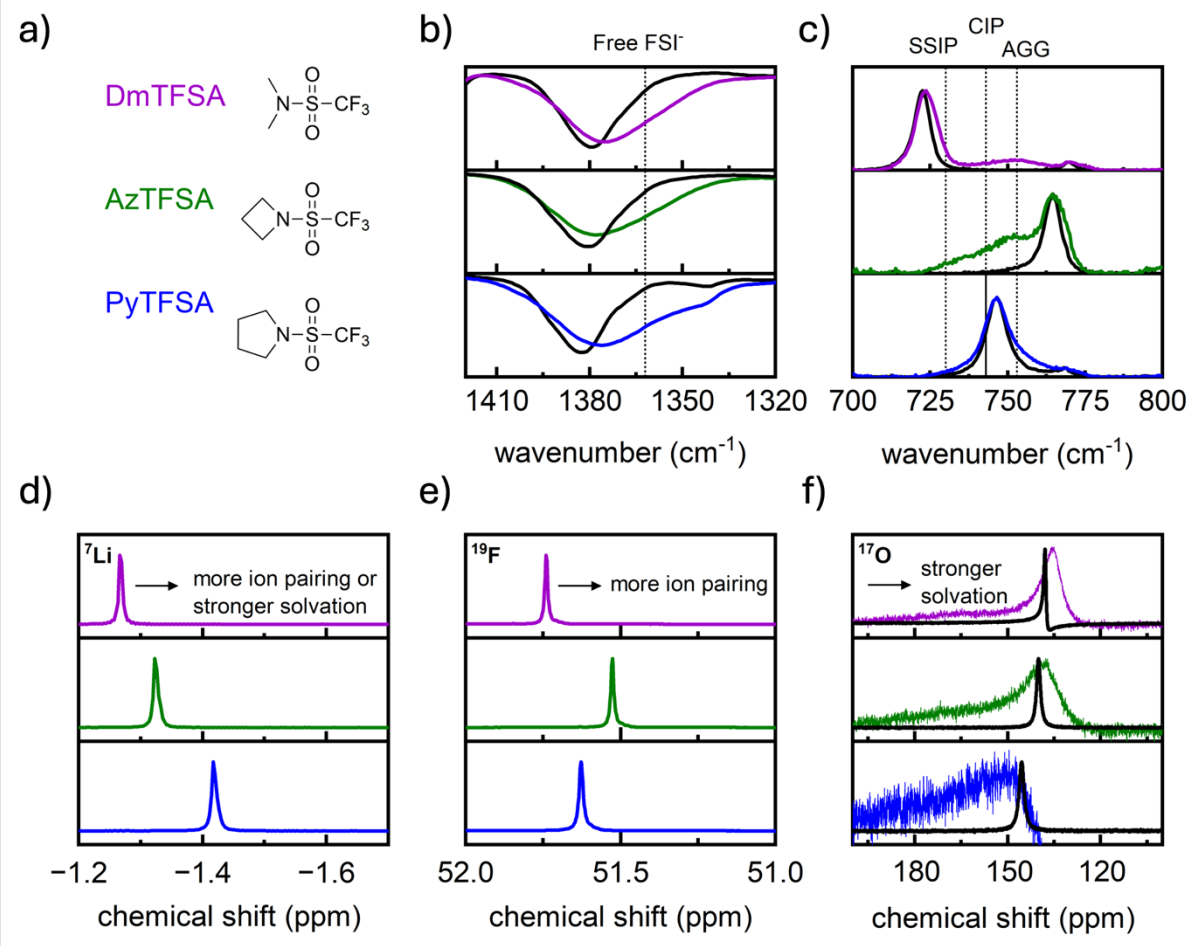

Figure 3. (a) Molecular structure of the investigated sulfonamide solvents. (b) FTIR spectra of different solvents and electrolytes. The black line corresponds to the pure solvent and the colored line to the mixed electrolyte. (c) Raman spectra of different solvents and electrolytes were obtained using a 785 nm laser. The black line corresponds to the pure solvent and the colored line to the mixed electrolyte. (d) ^{7}Li, (e) ^{19}F, and (f) ^{17}O NMR spectra of DmTFSA,

AzTFSA and PyTFSA. The intensities of the oxygen spectra were normalized. The black line corresponds to the pure solvent and the colored line to the mixed electrolyte.

Considering the Raman spectrum, FT-IR spectrum, and the ESP mapping of PyTFSA (Figure 3a), the larger upfield shift in the case of 1.6 M PyTFSA is attributed to stronger solvation of Li^+ by sulfonamide oxygen. In the case of 1.6 M DmTFSA and 1.6M AzTFSA, the relatively larger upfield shift of 1.6 M AzTFSA is attributed to enhanced Li^+-FSI^- contact in 1.6 M AzTFSA compared to 1.6 M DmTFSA owing to the combined steric and electronic effects. This interpretation agrees well with the Raman and FT-IR spectra. The ^{19}F-NMR (Figure 3e) in the LiFSI region (50-53 ppm) further confirms that 1.6 M AzTFSA shows more Li^+-FSI^- pairing than 1.6 M DmTFSA due to the relative upfield shift of 1.6 M AzTFSA. These findings are further confirmed by ^{17}O-NMR analysis (Figure 3f), which shows an upfield shift in the sulfonamide oxygen of 1.6 M DmTFSA compared to 1.6 M AzTFSA. 1.6 M PyTFSA shows a very broad peak with very low signal intensity after LiFSI salt is dissolved. This result could be due to the strong binding of Li^+ to the sulfonamide oxygen, which leads to a peak broadening. As the ESP values of AzTFSA and DmTFSA only differ by about 4 kJ/mol (Table S1), the increased ion pairing is, therefore, mostly created by the steric influence of the azetidine ring, which is small and rigid and does not allow bending of the molecule to accommodate Li^+ coordination. These findings further emphasize the impact of steric and electronic effects. The investigation of the solvation structure of the electrolytes confirms the

increased ion-pair formation in 1.6 M AzTFSA electrolyte, which explains its enhanced compatibility with Li metal anode.

NCM811 (9.3 mg/cm^2) full cells with 1.6 M DmTFSA and 1.6 M AzTFSA were tested to evaluate the effect of the electrolyte modifications in a practical cell setting. 20 μm Li on Cu foil was used as the anode (N/P = 2.5), and 20 μL of electrolyte for the full cells (Figure 4a). The cells were charged and discharged between 4.3 V and 3 V at 0.5C (1C = 188 mAh/g) with two formation cycles at 0.1C. The Li||NCM811 full cell with the 1.6 M LiFSI AzTFSA was able to cycle up to 150 cycles with 80% capacity retention at 0.5C. The superior performance of AzTFSA over DmTFSA and PyTFSA was attributed to the more efficient stabilization of the electrode-electrolyte interface.

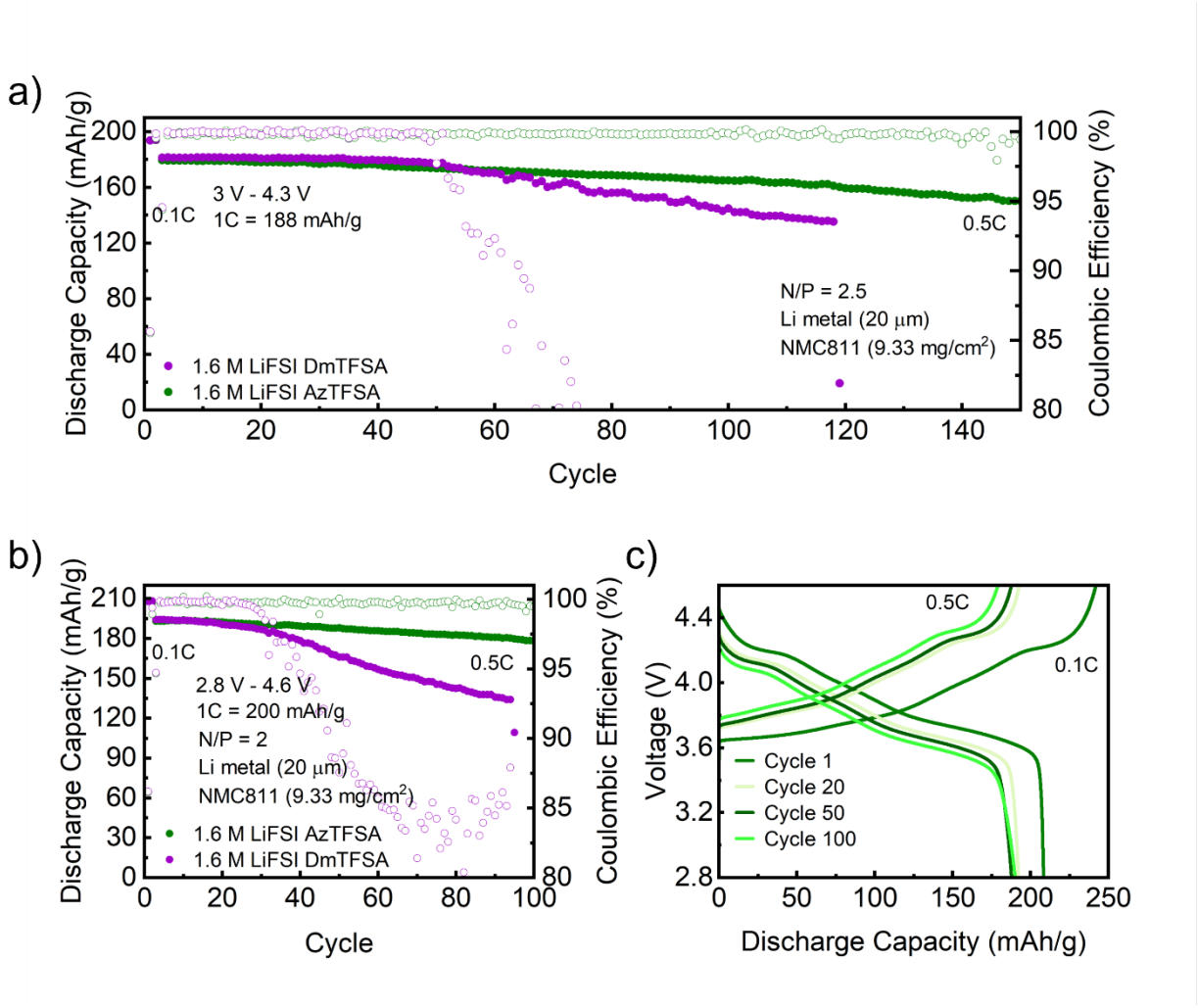

Figure 4. (a) Li-NMC811 full cell performance of 1.6 M DmTFSA and 1.6 M AzTFSA, cycled between 3 V and 4.3 V with 0.5C. (b) Li-NMC811 full cell performance of 1.6 M AzTFSA cycled between 2.8 V and 4.6 V with 0.5C. (c) Voltage trace of Li-NMC811 full cell performance of 1.6 M AzTFSA cycled between 2.8 V and 4.6 V with 0.5C.

To confirm the excellent high-voltage compatibility of 1.6 M AzTFSA electrolyte, full cells with NMC811 (9.3 mg/cm^2) and 20 μm Li on Cu foil as the anode (N/P ratio of 2) and 20 μL of electrolyte were cycled between 2.8 V and 4.6 V at 0.5C (1C = 200 mAh/g) with two activation cycles at 0.1C (Figure 4b). After 100 cycles, the corresponding full cell delivered a specific

capacity of 178.2 mAh/g and a capacity retention of 92%. The corresponding dQ/dV plot shows that after 100 cycles with a upper cutoff voltage of 4.6 V, the H2-H3 peak has not decayed in 1.6 M AzTFSA electrolyte (Figure S14).

The high intrinsic oxidative stability of the sulfonamide electrolyte (Figure 1b) coupled with an AGG-enriched solvation structure leads to an anion-derived CEI, which was verified by the deconvoluted XPS F1s spectrum obtained after 25 cycles, indicating high LiF content and homogeneous distribution along the depth (Figure S15a). The outer CEI shows S-F and LiF contributions, which can mainly be attributed to LiFSI decomposition[47, 48]. After 180 s of Ar sputtering, the inner CEI mainly consists of LiF. The S=O peak in the O1s spectrum, which can be attributed to salt decomposition, decreases in intensity after 180 s of sputtering, whereas the M-O peak increases, indicating the formation of a thin CEI (Figure S15b). XPS depth profile analysis was performed on the Li metal (20 μm) anode after cycling Li||NCM811 full cell. The full cell with 1.6 M AzTFSA was cycled for 25 cycles (Figure S16a-d) to probe the composition and homogeneity of the SEI. The surface XPS of the electrode suggests the preferential decomposition of LiFSI as well as the participation of the AzTFSA in the SEI formation. In the F1s spectrum at 0 s of Ar sputtering, the S-F (688.3 eV) contribution shows anion decomposition at the Li metal anode (Figure S16a). After 60 s of Ar sputtering, the F1s spectrum reveals high LiF content (684.6 eV), which is distributed homogenously along the depth. LiFSI decomposition is further confirmed by the S=O (532.3 eV) peak in the O1s spectrum and the SO_2F (170 eV, 168.82 eV) peak in the S2p spectrum (Figure S16b and S16d).

In the S2p spectra (Figure S16d), an obvious S_n^{2-} peak (161.5 eV, 162.3 eV) was observed for the 1.6 M AzTFSA, indicating a reduction of the anion at the surface, the intensity of which gradually decreased along the depth[48]. The C1s spectrum (Figure S16c) shows that the organic content of the SEI gradually decreased along the depth, which was accompanied by an increase in the content of inorganic species. We also observed an increase in the Li_2O (528.2 eV) content along the depth of the SEI. These results suggest the formation of a stable, bilayer SEI structure with an inorganic-rich inner layer and an outer organic layer, thus explaining the improved Li metal compatibility of the 1.6 M AzTFSA through solvation structure engineering.

In summary, we demonstrated the rational design of fluorinated sulfonamide solvents by tuning the substituent at the N-terminus to optimize the Li^+ solvation structure and boost electrochemical performance. We also demonstrated the critical role of steric and electronic effects to favor CIP and AGG formation in weakly coordinating electrolytes over solvent-separated ion pairs, SSIPs. This leads to improved Li metal compatibility and high voltage stability, enabling stable operation under challenging conditions at high voltage in a Li-NMC811 full cell using a single salt solvent electrolyte. This work highlights that solvation structure engineering by increasing ion-pairing through steric and electronic control can be outside the traditional substrate scope of ethers. Furthermore, it gives insight into the complex structure-property relationship of salt-like solvents with different cyclic amine substituents.

ASSOCIATED CONTENT

The supporting information free of charge at

Experimental details, NMR spectra, electrolyte properties, Raman spectra, FT-IR spectra, CE profiles, voltage-time profiles, CV, EIS, XPS and SEM images

AUTHOR INFORMATION

Corresponding Authors

Ali Coskun – Department of Chemistry, University of Fribourg, Fribourg 1700, Switzerland; orcid.org/0000- 0002-4760-1546;

Email: ali.coskun@unifr.ch

Jang Wook Choi – School of Chemical and Biological Engineering, Department of Materials Science and Engineering, and Institute of Chemical Processes, Seoul National University, Gwanak-gu, Seoul 08826, Republic of Korea; orcid.org/0000-0001-8783-0901;

Email: jangwookchoi@snu.ac.kr

Authors

Lea Pompizii – Department of Chemistry, University of Fribourg, Chemin de Musee 9, Fribourg 1700, Switzerland

Mingliang Liu – Department of Chemistry, University of Fribourg, Chemin de Musee 9, Fribourg 1700, Switzerland

Leonie Braks – Department of Chemistry, University of Fribourg, Chemin de Musee 9, Fribourg 1700, Switzerland

Timur Ashirov – Department of Chemistry, University of Fribourg, Chemin de Musee 9, Fribourg 1700, Switzerland

Tianhong Zhou – Department of Chemistry, University of Fribourg, Chemin de Musee 9, Fribourg 1700, Switzerland

Mounir Mensi – Institute of Chemical Sciences and Engineering (ISIC), École Polytechnique Fédérale de Lausanne, Sion, 1950, Switzerland

Dongmin Park – School of Chemical and Biological Engineering, Seoul National University, Gwanak-gu, Seoul 08826, Republic of Korea

Notes

"The authors declare no competing financial interest."

ACKNOWLEDGMENT

A.C. and J.W.C. acknowledge the support from the Swiss National Science Foundation (SNF) (Sinergia, CRSII5_202296).

REFERENCES

(1) Bruce, P. G.; Freunberger, S. A.; Hardwick, L. J.; Tarascon, J.-M. Li–O2 and Li–S batteries with high energy storage. Nat. Materials 2012, 11 (1), 19-29.

(2) Zhang, J. G.; Xu, W.; Xiao, J.; Cao, X.; Liu, J. Lithium Metal Anodes with Nonaqueous Electrolytes. Chem. Rev. 2020, 120 (24), 13312-13348.

(3) Zhao, Y.; Zhou, T.; Mensi, M.; Choi, J. W.; Coskun, A. Electrolyte engineering via ether solvent fluorination for developing stable non-aqueous lithium metal batteries. Nat. Commun. 2023, 14 (1), 299.

(4) Choi, J. W.; Aurbach, D. Promise and reality of post-lithium-ion batteries with high energy densities. Nat. Rev. Mater. 2016, 1 (4), 16013.

(5) Lin, D.; Liu, Y.; Cui, Y. Reviving the lithium metal anode for high-energy batteries. Nat. Nanotechnol. 2017, 12 (3), 194-206.

(6) Zheng, X.; Huang, L.; Ye, X.; Zhang, J.; Min, F.; Luo, W.; Huang, Y. Critical effects of electrolyte recipes for Li and Na metal batteries. Chem 2021, 7 (9), 2312-2346.

(7) Zhang, X.; Yang, Y.; Zhou, Z. Towards practical lithium-metal anodes. Chem. Soc. Rev. 2020, 49 (10), 3040-3071.

(8) Kim, H.; Jeong, G.; Kim, Y.-U.; Kim, J.-H.; Park, C.-M.; Sohn, H.-J. Metallic anodes for next generation secondary batteries. Chem. Soc. Rev. 2013, 42 (23), 9011.

(9) Wang, H.; Yu, Z.; Kong, X.; Kim, S. C.; Boyle, D. T.; Qin, J.; Bao, Z.; Cui, Y. Liquid electrolyte: The nexus of practical lithium metal batteries. Joule 2022, 6 (3), 588-616.

(10) Chen, Y.; Yu, Z.; Rudnicki, P.; Gong, H.; Huang, Z.; Kim, S. C.; Lai, J. C.; Kong, X.; Qin, J.; Cui, Y.; et al. Steric Effect Tuned Ion Solvation Enabling Stable Cycling of High-Voltage Lithium Metal Battery. J. Am. Chem. Soc. 2021, 143 (44), 18703-18713.

(11) Zhao, Y.; Zhou, T.; Jeurgens, L. P. H.; Kong, X.; Choi, J. W.; Coskun, A. Electrolyte engineering for highly inorganic solid electrolyte interphase in high-performance lithium metal batteries. Chem 2023, 9 (3), 682-697.

(12) Fan, X.; Wang, C. High-voltage liquid electrolytes for Li batteries: progress and perspectives. Chem. Soc. Rev. 2021, 50 (18), 10486-10566.

(13) Yu, L.; Chen, S.; Lee, H.; Zhang, L.; Engelhard, M. H.; Li, Q.; Jiao, S.; Liu, J.; Xu, W.; Zhang, J.-G. A Localized High-Concentration Electrolyte with Optimized Solvents and Lithium Difluoro(oxalate)borate Additive for Stable Lithium Metal Batteries. ACS Energy Lett. 2018, 3 (9), 2059-2067.

(14) Xu, K. Nonaqueous Liquid Electrolytes for Lithium-Based Rechargeable Batteries. Chem. Rev. 2004, 104 (10), 4303-4418.

(15) Zhao, Y.; Zhou, T.; Ashirov, T.; Kazzi, M. E.; Cancellieri, C.; Jeurgens, L. P. H.; Choi, J. W.; Coskun, A. Fluorinated ether electrolyte with controlled solvation structure for high voltage lithium metal batteries. Nat. Commun. 2022, 13 (1), 2575.

(16) Ren, X.; Chen, S.; Lee, H.; Mei, D.; Engelhard, M. H.; Burton, S. D.; Zhao, W.; Zheng, J.; Li, Q.; Ding, M. S.; et al. Localized High-Concentration Sulfone Electrolytes for High-Efficiency Lithium-Metal Batteries. Chem 2018, 4 (8), 1877-1892.

(17) Xue, W.; Huang, M.; Li, Y.; Zhu, Y. G.; Gao, R.; Xiao, X.; Zhang, W.; Li, S.; Xu, G.; Yu, Y.; et al. Ultra-high-voltage Ni-rich layered cathodes in practical Li metal batteries enabled by a sulfonamide-based electrolyte. Nat. Energy 2021, 6 (5), 495-505.

(18) Feng, S.; Huang, M.; Lamb, J. R.; Zhang, W.; Tatara, R.; Zhang, Y.; Zhu, Y. G.; Perkinson, C. F.; Johnson, J. A.; Shao-Horn, Y. Molecular Design of Stable Sulfamide- and Sulfonamide-based Electrolytes for Aprotic Li-O(2) Batteries. Chem 2019, 5 (10), 2630-2641.

(19) Dong, L.; Zhong, S.; Yuan, B.; Ji, Y.; Liu, J.; Liu, Y.; Yang, C.; Han, J.; He, W. Electrolyte Engineering for High-Voltage Lithium Metal Batteries. Research 2022, 9837586.

(20) Li, T.; Zhang, X.-Q.; Shi, P.; Zhang, Q. Fluorinated Solid-Electrolyte Interphase in High-Voltage Lithium Metal Batteries. Joule 2019, 3 (11), 2647-2661.

(21) Ren, X.; Gao, P.; Zou, L.; Jiao, S.; Cao, X.; Zhang, X.; Jia, H.; Engelhard, M. H.; Matthews, B. E.; Wu, H.; et al. Role of inner solvation sheath within salt–solvent complexes in tailoring electrode/electrolyte interphases for lithium metal batteries. Proc. Natl. Acad. Sci. U. S. A. 2020, 117 (46), 28603-28613.

(22) Ma, M.; Huang, R.; Ling, M.; Hu, Y. S.; Pan, H. Towards stable electrode–electrolyte interphases: Regulating solvation structures in electrolytes for rechargeable batteries. Interd. Mater. 2023, 2 (6), 833-854.

(23) Park, E.; Park, J.; Lee, K.; Zhao, Y.; Zhou, T.; Park, G.; Jeong, M.-G.; Choi, M.; Yoo, D.-J.; Jung, H.-G.; et al. Exploiting the Steric Effect and Low Dielectric Constant of 1,2-Dimethoxypropane for 4.3 V Lithium Metal Batteries. ACS Energy Lett. 2022, 8 (1), 179-188.

(24) Chen, S.; Zheng, J.; Mei, D.; Han, K. S.; Engelhard, M. H.; Zhao, W.; Xu, W.; Liu, J.; Zhang, J. G. High-Voltage Lithium-Metal Batteries Enabled by Localized High-Concentration Electrolytes. Adv. Mater. 2018, 30 (21), 1706102.

(25) Miao, R.; Yang, J.; Xu, Z.; Wang, J.; Nuli, Y.; Sun, L. A new ether-based electrolyte for dendrite-free lithium-metal based rechargeable batteries. Sci. Rep. 2016, 6, 21771.

(26) Yamada, Y.; Yaegashi, M.; Abe, T.; Yamada, A. A superconcentrated ether electrolyte for fast-charging Li-ion batteries. Chem. Commun. 2013, 49 (95), 11194.

(27) Amanchukwu, C. V.; Yu, Z.; Kong, X.; Qin, J.; Cui, Y.; Bao, Z. A New Class of Ionically Conducting Fluorinated Ether Electrolytes with High Electrochemical Stability. J. Am. Chem. Soc. 2020, 142 (16), 7393-7403.

(28) Wang, J.; Yamada, Y.; Sodeyama, K.; Chiang, C. H.; Tateyama, Y.; Yamada, A. Superconcentrated electrolytes for a high-voltage lithium-ion battery. Nat. Commun. 2016, 7 (1), 12032.

(29) Cao, X.; Jia, H.; Xu, W.; Zhang, J.-G. Review—Localized High-Concentration Electrolytes for Lithium Batteries. J. Electrochem. Soc. 2021, 168 (1), 010522.

(30) Kim, M.; An, J.; Shin, S.-J.; Hwang, I.; Lee, J.; Park, Y.; Kim, J.; Park, E.; Kim, J.; Park, G.; et al. Anti-corrosive electrolyte design for extending the calendar life of lithium metal batteries. Energy Environ. Sci. 2024, 17 (16), 6079-6090.

(31) Yao, Y. X.; Chen, X.; Yan, C.; Zhang, X. Q.; Cai, W. L.; Huang, J. Q.; Zhang, Q. Regulating Interfacial Chemistry in Lithium-Ion Batteries by a Weakly Solvating Electrolyte**. Angew. Chem. Int. Ed. 2021, 60 (8), 4090-4097.

(32) Li, Z.; Rao, H.; Atwi, R.; Sivakumar, B. M.; Gwalani, B.; Gray, S.; Han, K. S.; Everett, T. A.; Ajantiwalay, T. A.; Murugesan, V.; et al. Non-polar ether-based electrolyte solutions for stable high-voltage non-aqueous lithium metal batteries. Nat. Commun. 2023, 14 (1), 868.

(33) Mominur Rahman, M.; Hu, E. Electron Delocalization Enables Sulfone-based Single-solvent Electrolyte for Lithium Metal Batteries. Angew. Chem. Int. Ed. 2023, 62 (44), e202311051.

(34) Lee, K.; Kwon, S.-H.; Kim, J.; Park, E.; Kim, I.; Ahn, H. C.; Coskun, A.; Choi, J. W. Fluorinated Cyclic Ether Diluent for High-Voltage Lithium Metal Batteries. ACS Energy Lett. 2024, 9 (5), 2201-2211.

(35) Zhang, H.; Zeng, Z.; Ma, F.; Wu, Q.; Wang, X.; Cheng, S.; Xie, J. Cyclopentylmethyl Ether, a Non-Fluorinated, Weakly Solvating and Wide Temperature Solvent for High-Performance Lithium Metal Battery. Angew. Chem. Int. Ed. 2023, 62 (21), e202300771.

(36) Xue, W.; Gao, R.; Shi, Z.; Xiao, X.; Zhang, W.; Zhang, Y.; Zhu, Y. G.; Waluyo, I.; Li, Y.; Hill, M. R.; et al. Stabilizing electrode–electrolyte interfaces to realize high-voltage Li||$LiCoO_2$ batteries by a sulfonamide-based electrolyte. Energy Environ. Sci. 2021, 14 (11), 6030-6040.

(37) Xue, W.; Shi, Z.; Huang, M.; Feng, S.; Wang, C.; Wang, F.; Lopez, J.; Qiao, B.; Xu, G.; Zhang, W.; et al. FSI-inspired solvent and “full fluorosulfonyl” electrolyte for 4 V class lithium-metal batteries. Energy Environ. Sci. 2020, 13 (1), 212-220.

(38) Sun, C.; Li, R.; Weng, S.; Zhu, C.; Chen, L.; Jiang, S.; Li, L.; Xiao, X.; Liu, C.; Chen, L.; et al. Reduction-Tolerance Electrolyte Design for High-Energy Lithium Batteries. Angew. Chem. Int. Ed. 2024, 63 (19), e202400761.

(39) Kim, S.; Jeon, J. H.; Park, K.; Kweon, S. H.; Hyun, J. H.; Song, C.; Lee, D.; Song, G.; Yu, S. H.; Lee, T. K.; et al. Electrolyte Design for High-Voltage Lithium-Metal Batteries with Synthetic Sulfonamide-Based Solvent and Electrochemically Active Additives. Adv. Mater. 2024, 36 (24), 2401615.

(40) Zhang, G.; Li, J.; Wang, Q.; Wang, H.; Wang, J.; Yu, K.; Chang, J.; Wang, C.; Hong, X.; Ma, Q.; et al. A Nonflammable Electrolyte for High-Voltage Lithium Metal Batteries. ACS Energy Lett. 2023, 8 (7), 2868-2877.

(41) Adams, B. D.; Zheng, J.; Ren, X.; Xu, W.; Zhang, J. G. Accurate Determination of Coulombic Efficiency for Lithium Metal Anodes and Lithium Metal Batteries. Adv. Energy Mater. 2017, 8 (7).

(42) Jafta, C. J.; Sun, X. G.; Lyu, H.; Chen, H.; Thapaliya, B. P.; Heller, W. T.; Cuneo, M. J.; Mayes, R. T.; Paranthaman, M. P.; Dai, S.; et al. Insight into the Solid Electrolyte Interphase Formation in Bis(fluorosulfonyl)Imide Based Ionic Liquid Electrolytes. Adv. Funct. Mater. 2021, 31 (23), 2008708.

(43) Quan, Y.; Li, S.; Zhang, N.; Cui, X.; Zhao, D.; Zhang, Y.; Wang, M.; Li, X. Improving performances of cathode-electrolyte interphase via the potentiostatic reduction of lithium bis(fluorosulfonyl)imide additive. Electrochim. Acta 2023, 460.

(44) Ding, J. F.; Xu, R.; Yao, N.; Chen, X.; Xiao, Y.; Yao, Y. X.; Yan, C.; Xie, J.; Huang, J. Q. Non-Solvating and Low-Dielectricity Cosolvent for Anion-Derived Solid Electrolyte Interphases in Lithium Metal Batteries. Angew. Chem. Int. Ed. 2021, 60 (20), 11442-11447.

(45) Alvarado, J.; Schroeder, M. A.; Zhang, M.; Borodin, O.; Gobrogge, E.; Olguin, M.; Ding, M. S.; Gobet, M.; Greenbaum, S.; Meng, Y. S.; et al. A carbonate-free, sulfone-based electrolyte for high-voltage Li-ion batteries. Mater. Today 2018, 21 (4), 341-353.

(46) Zhao, Y.; Zhou, T.; El Kazzi, M.; Coskun, A. Fluorinated Cyclic Ether Co-solvents for Ultra-high-Voltage Practical Lithium-Metal Batteries. ACS Appl. Energy Mater. 2022, 5 (6), 7784-7790.

(47) Beyene, T. T.; Bezabh, H. K.; Weret, M. A.; Hagos, T. M.; Huang, C.-J.; Wang, C.-H.; Su, W.-N.; Dai, H.; Hwang, B.-J. Concentrated Dual-Salt Electrolyte to Stabilize Li Metal and Increase Cycle Life of Anode Free Li-Metal Batteries. J. Electrochem. Soc. 2019, 166 (8), A1501-A1509.

(48) Cao, X.; Ren, X.; Zou, L.; Engelhard, M. H.; Huang, W.; Wang, H.; Matthews, B. E.; Lee, H.; Niu, C.; Arey, B. W.; et al. Monolithic solid–electrolyte interphases formed in fluorinated orthoformate-based electrolytes minimize Li depletion and pulverization. Nat. Energy 2019, 4 (9), 796-805.